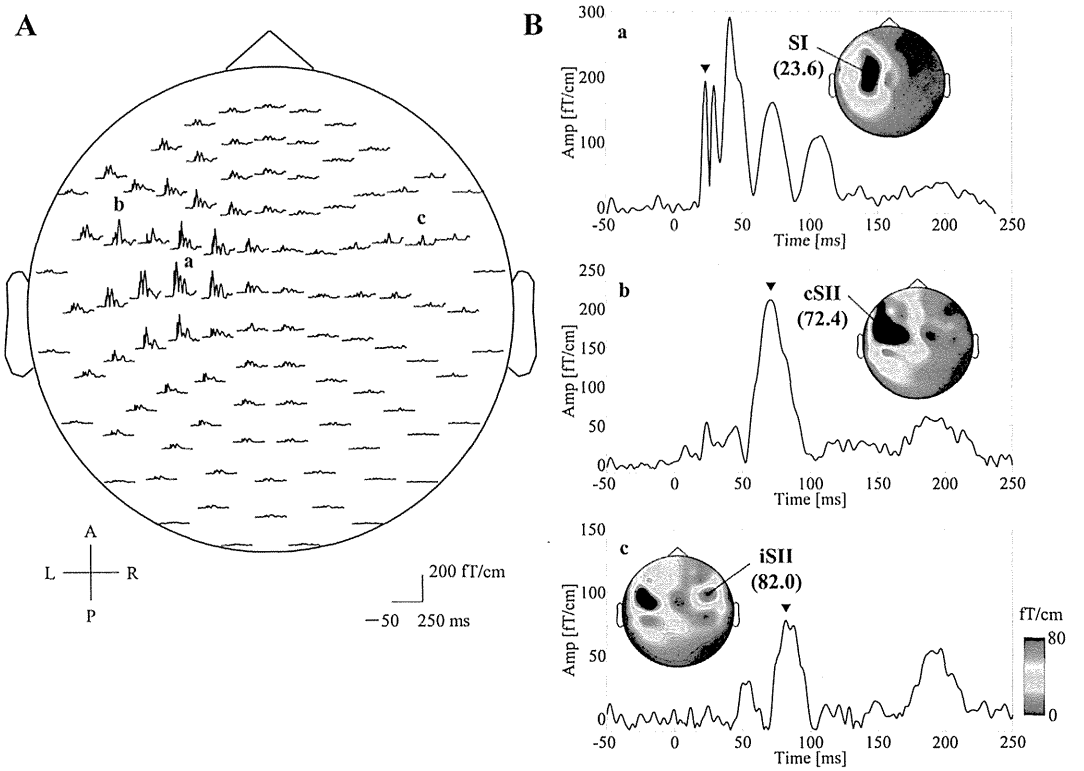

Fig. 2. SEFs in a representative old subject. (A) A plot of all sensors. As in Fig. 1A, small letters (i.e., a, b, c) represent the sensors showing maximal amplitudes for SI, cSII, iSII, respectively. (B) Enlarged figures for the sensors indicated by the small letters and each isocontour map at peak latency. This subject shows increased amplitude of N20m as well as shortened peak latencies for the bilateral SII responses. The waveforms of SII show shorter duration without a change in the onset.

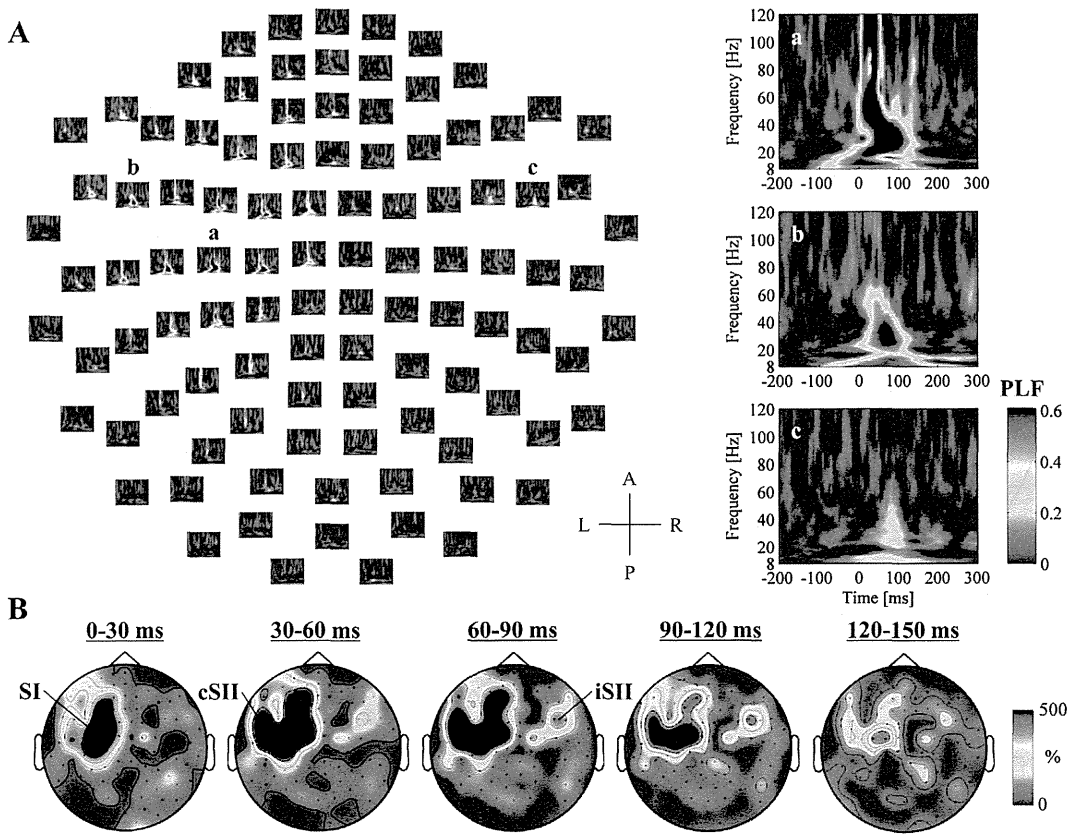

Fig. 3. PLF analysis in a representative old subject. (A) A plot of all sensors. Small letters indicate representative sensors for SI, cSII, and iSII, respectively, which correspond to the sensors determined on the SEF analysis. Enlarged figures on the right show PLFs at each area. (B) Time-course of isocontour field distribution summed for 8–50 Hz. Note that the strengths of activity are expressed as a relative ratio with respect to the baseline period at each sensor.

relatively lower in frequency and value. The activities lasted up to 200 ms in both areas, peaking at around the time of maximal amplitudes of SEFs in each area (Fig. 3A and B). In a group comparison, the PLFs of both SI and SII were significantly increased in the old subjects (Fig. 4, left and middle columns). The point-by-point *t*-tests showed significant differences in the entire time–frequency range of the observed activity in SI and cSII (Fig. 4, right column, top and middle). Since the significant points were distributed in a contiguous manner ranging from alpha to gamma band in both areas, we defined ROIs as follows: 8–120 Hz and 0–200 ms for SI, and 8–60 Hz and 0–200 ms for cSII. We performed the group comparison using mean values of a contiguous region within the ROIs, and verified the significance in SI ($p < 0.001$). Likewise, PLF of cSII was significantly increased in the old ($p < 0.01$). Concerning iSII, the increase was significant in a restricted region within the gamma-frequency band, ranging from 35 to 50 Hz within 65–135 ms of the post-stimulus period (Fig. 4, right column, bottom). Group comparison using means of contiguous values within the ROI confirmed a significant increase in the old subjects ($p < 0.01$).

3.4. wPLIs between SI and SII

In the wPLI analysis, we identified a significantly correlated activities between SI and SII (Fig. 5A and B). The increase of wPLI was observed within 200 ms following the stimulus onset with an identical time-course to SEFs and PLFs, and the frequency spanned broadly, ranging from alpha to gamma band. Despite the close proximity of cSII to SI, the synchronous activities in the two regions were well separated (Fig. 5C). Overall, the activities were relatively low in the young subjects, whereas the old subjects showed overt activities (Fig. 6, left and middle columns). In view of the difference in frequency and time window between the groups, we set the time–frequency ROIs as follows: 8–13 Hz and −100–150 ms for SI–cSII (Fig. 6, right column, top), 8–50 Hz and 0–200 ms for SI–iSII (Fig. 6, right column, middle), 8–50 Hz and 0–125 ms for cSII–iSII (Fig. 6, right column, bottom). Consequently, mean values obtained from the contiguous time–frequency regions proved significant increase in the old subjects for all comparisons ($p < 0.001$ for SI–iSII and cSII–iSII, $p < 0.01$ for SI–cSII).

4. Discussion

The current study provides the electrophysiological evidence of age-related changes within the somatosensory areas. We demonstrated the age-related changes both in SI and SII by conventional SEF analysis as well as the measures of synchronous oscillatory activities. In particular, the most novel finding of this study is that the age-related changes occur outside SI, namely in SII. PLF measures local field synchrony, while wPLI reflects functional connectivity between the two cortical areas. Thus, age-related changes are profound across the somatosensory areas with interaction between each other. We discuss each finding in detail in the following sections.

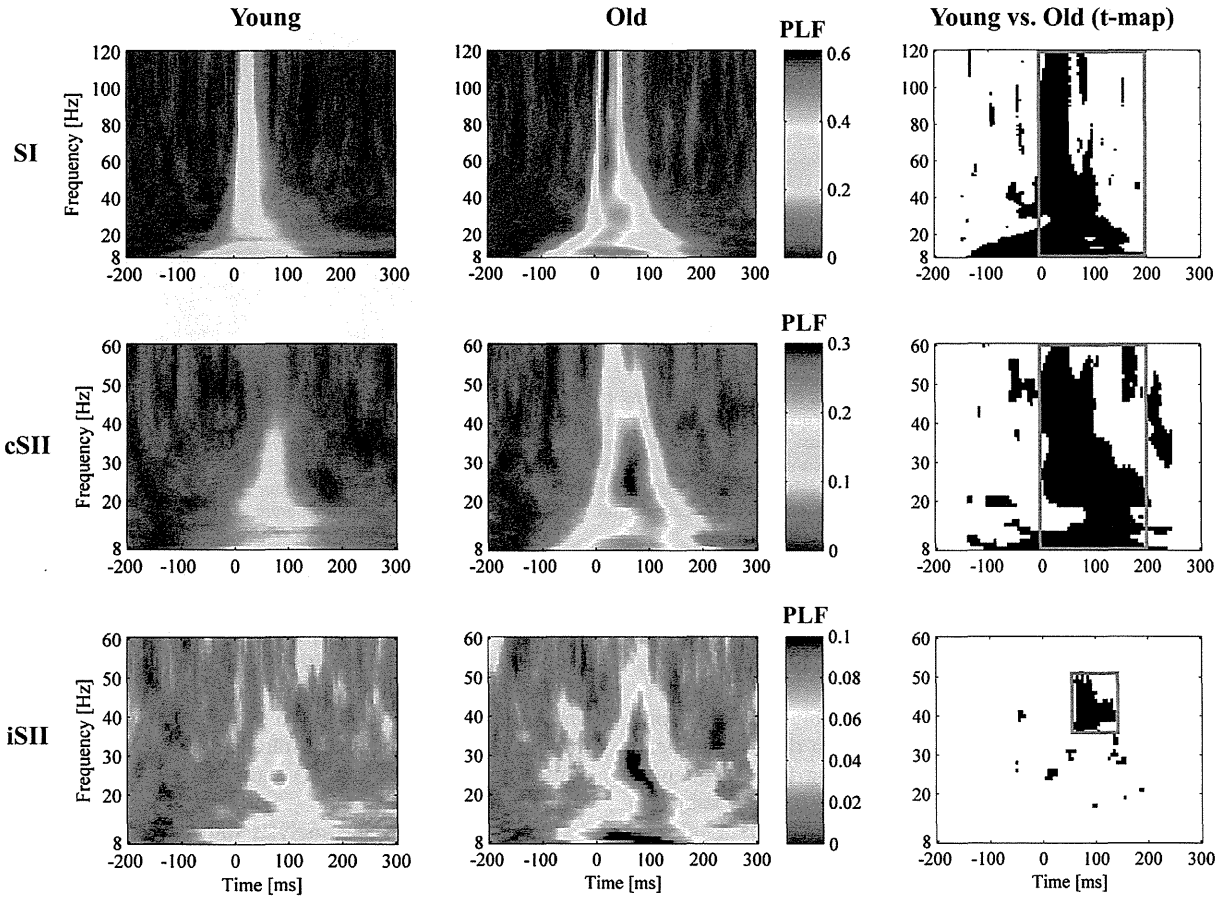

Fig. 4. Grand-means for PLFs in young (left column) and old (middle column) subjects, and point-by-point *t*-test results for PLFs (right column). Red rectangles mark the time–frequency ROIs as defined in the text. Note that only the statistically significant points ($p < 0.05$) are displayed in the *t*-maps. PLFs are significantly increased in the old subjects: PLFs in SI and cSII show significant differences in the entire frequency range and time course, whereas those in iSII show a significant increase in the gamma-frequency band.

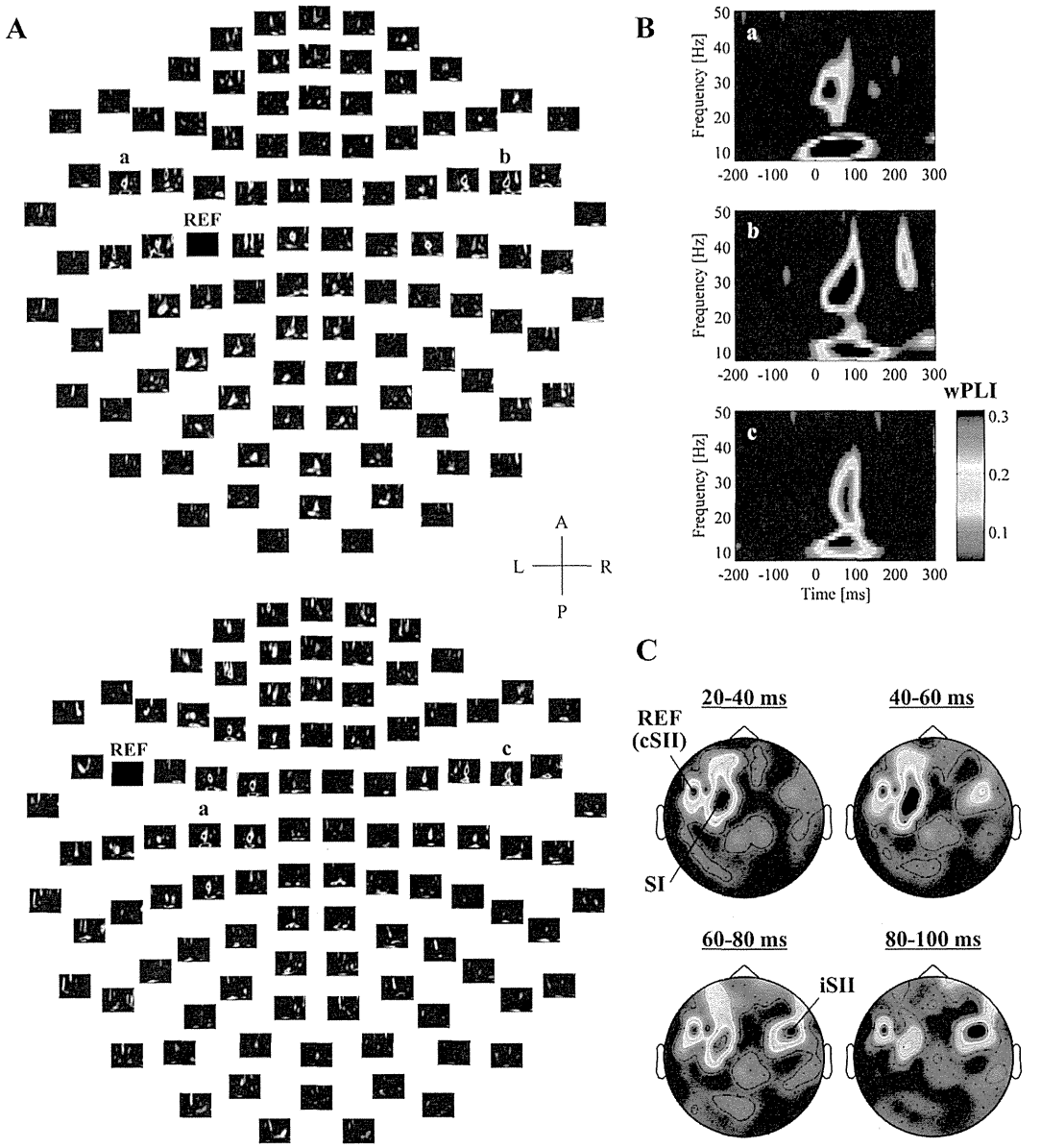

Fig. 5. wPLI analysis in a representative old subject. (A) A plot of all sensors. The sensor for SI activity is used as a reference sensor in the upper figure, whereas the sensor for cSII activity is used as a reference in the lower figure. The sensors indicated by the small letters show robust coherent activity with respect to the reference sensors, indicating significant phase correlation among the somatosensory areas. Coherent activities are observed in relatively broader areas when SI is used as a reference. This may be attributable to additional coherent activities in adjacent areas such as the posterior parietal cortex. In contrast, robust coherent activities between SI and SII can be well depicted when cSII is referenced. (B) Enlarged figures show each sensor indicated by the letters. (C) Time-course of the isocontour field distribution for the coherent activity within 8–40 Hz. Here, a sensor for cSII is set as the reference for the wPLI computation. Note that SI, cSII, and iSII show coherent activities in a non-contiguous fashion.

4.1. Age-related changes in major components of SEFs

With respect to SI, we found significantly increased amplitude of N20m in the old, which was well consistent with the previous reports using SEP and SEF (Drechsler, 1978; Huttunen et al., 1999; Stephen et al., 2006). This finding is probably caused by cortical disinhibition in SI that is closely related to the intracortical inhibitory mechanism. An SEP study examining high frequency oscillations (HFOs) in humans has demonstrated that old subjects exhibited enhancement of the later peaks of HFOs (Nakano and Hashimoto, 1999), which is linked to the GABAergic interneuronal inhibitory mechanism within SI (Hashimoto et al., 1996; Hashimoto, 2000; Ozaki and Hashimoto, 2011). In functional respect, age-related expansion of the hand representation has been observed in humans (Kalisch et al., 2009). A higher threshold for spatial discrimination in the old (Dinse et al., 2006) was shown to be significantly correlated with the enlarged hand representation, which resulted from the decreased inhibition within SI (Kalisch et al., 2009). Thus, there is an ample body of evidence to support the disinhibition in SI. Our results also showed that the latency of N20m was prolonged in the old, which is a reasonable finding in normal aging due to the slowing of conduction velocity in the periphery. Since the prolongation was significant even after adjusting for height, it would underpin the presence of age-related changes in our subjects.

Interestingly, the SEF analysis showed that the latencies of SII were significantly shortened in the old subjects. This was an unexpected finding given the slowing of conduction velocity in the afferent inputs. The latency that we measured in this study was the peak latency of the major component of SII. A careful inspection of the waveforms revealed that they were steeper in the old than in the young without affecting the onset latency. Thus, our

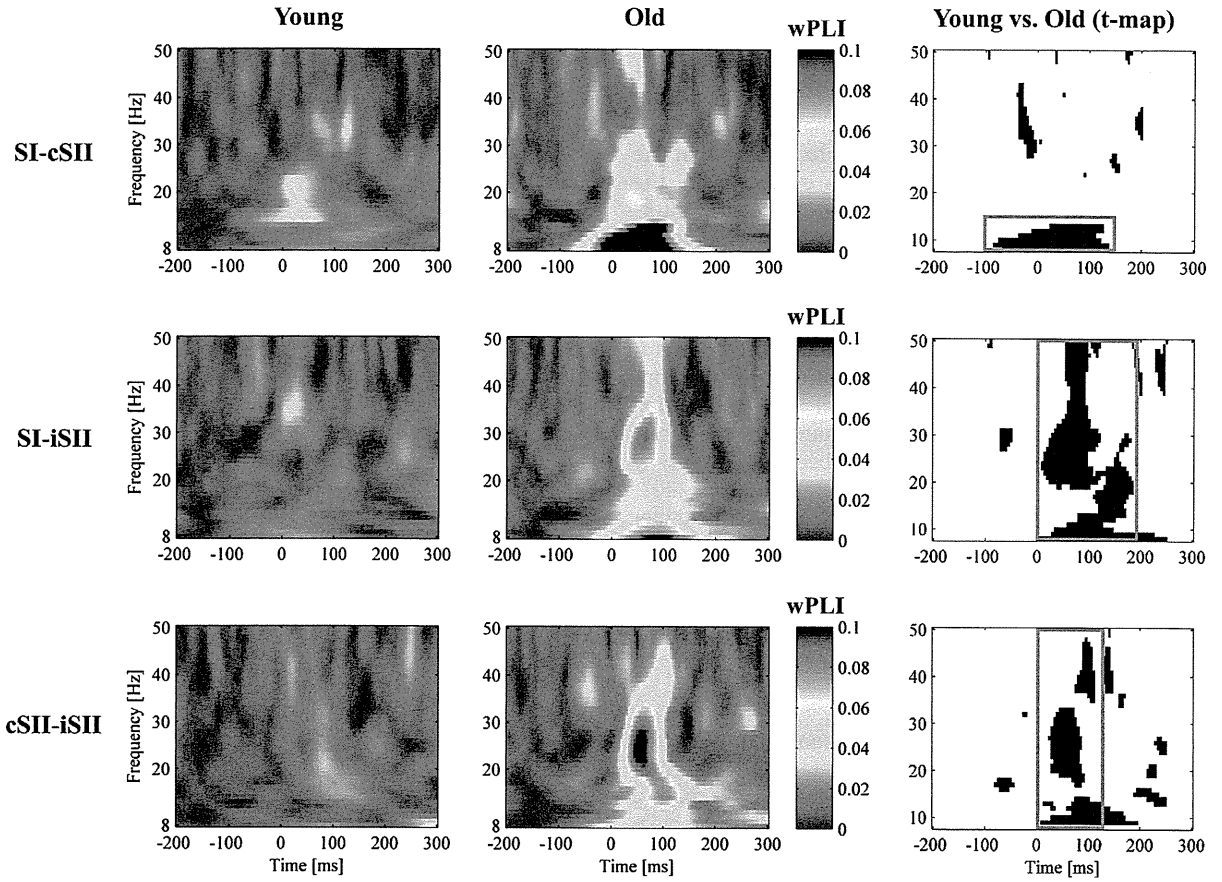

Fig. 6. Grand-means for wPLIs in young (left column) and old (middle column) subjects, and point-by-point *t*-test results for wPLI (right column). Red rectangles mark the ROIs as defined in the text. Only statistically significant points ($p < 0.05$) are displayed in the *t*-maps. The old subjects show significantly elevated wPLIs in each comparison.

finding suggests faster excitation rather than earlier excitation in SII. Enhanced cortical excitability may lead to higher amplitude, but amplitude difference between the two groups did not reach a significant level probably due to the problem with source-to-sensor distance. However, the PLF analysis discussed in Section 4.2 provides supportive findings in consolidating the age-related changes in cortical excitability in SII.

4.2. Age-related changes across SI and SII evidenced by the phase analysis

As emphasized in Section 2, PLF and wPLI are independent of the amplitudes of original signals and purely reflect information about the phase. Thus, we can provide meaningful results about the age-related changes in SI and SII by analyzing both local and inter-areal oscillatory activities using those indices. First, the PLF analysis showed substantial changes in local field synchrony in each cortical area. The age-related increase of PLF in SI well consolidates the cortical disinhibition in connection with the increased N20m amplitude, which alone might not be sufficient for proving the enhanced activity, considering the influence of distance. More importantly, we could demonstrate the enhanced local synchrony in SII, as evidenced by the increased PLF in bilateral SIIs. This finding is also consistent with SEFs of SII, in which the shortened peak latency in conjunction with steeper waveforms was suggestive of enhanced synchrony in its activity. Although the amplitudes were not significantly different in the SEF analysis, PLF was more successful in consolidating the magnitude of excitability in SII, probably by overcoming the issue of source-to-sensor distance. The PLF of cSII may be affected by its proximity to SI, which showed prominent activity in the old subjects (i.e., volume conduction effect). However, iSII was well isolated from SI so that the analysis of iSII region was unaffected by the enhanced SI activity. Since the PLF of iSII was significantly increased in the old, it is likely that cSII also shows increased PLF due to its closer relationship with SI. Therefore, we provide solid evidence for enhanced cortical excitability in SII. Secondly, we demonstrated the significantly enhanced functional interaction between SI and SII in the wPLI analysis. We used wPLI, but no other coherence measures, to ensure not to analyze synchrony between the signals with the same source (i.e., common source problem). Consequently, the functional correlation was evident in the alpha to gamma frequency band, which is consistent with the previous studies using the phase-locking value (PLV) (Hagiwara et al., 2010; Simões et al., 2003). Despite the spreading activity of SI to the adjacent cSII region, especially in the old, the wPLI analysis was successful in delineating meaningful synchrony between SI and cSII. This is not surprising because the original report of wPLI demonstrated truly coherent activity with an even closer distance of neighboring sensors, as in the setting of local field potential measurement (Vinck et al., 2011). The lower wPLI values, especially in the young subjects, may be attributable to methodological differences between wPLI and PLV. PLV weighs a synchronicity of oscillations with zero phase-delay as maximal value, whereas wPLI takes up synchronous activity with consistent phase-lag while dismissing the zero phase-lag components as the volume conduction or common source effect. Thus, the false positive rate is minimized in the wPLI analysis while the level of specificity is maximized. In addition, the absence of any task-related effects can be related to the low wPLI values. The lack of significant increase in high-frequency activity between SI and cSII may also be attributable to the same reasons. However, even taking that into account, it

may still be questionable whether the wPLI values correspond to all physiological phenomena for functional connectivity. However, since the relative increase of coherent activities is valid on the basis of the statistically significant increment of wPLI, it is clear that the old subjects showed an enhanced functional interaction between SI and SII. Additionally, it is reasonable to assume that the disinhibition of the activities in SI and SII as evidenced by the PLF analysis resulted in disinhibition of the cortico–cortical interaction. Another possible reason for the increased functional interaction, which we should mention, is a plastic-adaptive process in SII. Lesion studies in animals demonstrated that the inactivation of the SII cortex resulted in reduced activity of SI neurons (Turman et al., 1995; Zhang et al., 2001a). In humans, a study using transcranial magnetic stimulation (Raij et al., 2008) also suggested top-down modulation from SII to SI. The reciprocal SI–SII interaction in early-stage somatosensory processing is achieved by the direct thalamocortical pathway to SII, which has been suggested by numerous studies (Karhu and Tesche, 1999; Lin and Forss, 2002; Raij et al., 2008; Zhang et al., 1996, 2001a, 2001b). Thus, the higher PLF as well as wPLI in the old might reflect age-related changes in top-down gain-control function. However, we must admit that this possibility remains speculative in the current study.

4.3. Limitations of this study

Although orientation of the cortical activation is an important factor in MEG, the cortical current of SII shows tangential orientation similar to SI. Thus, orientation related issue does not make a significant difference between SI and SII. However, amplitude measurements in MEG can vary, depending on the distance between the source of activity and sensors. Specifically, here, distance encompasses two factors: *anatomical distance* means the depth within the brain, and *spatial distance* that represents the physical distance between the scalp and sensor array. The *anatomical distance* significantly affects the MEG sensor sensitivity. In contrast to SI, SII is located deep in the parietal operculum in the Sylvian fissure. This is the reason why direct recording of SII activity can only be achieved using stereotactic placement of depth electrodes (Barba et al., 2002; Mazzola et al., 2006). Another important issue in MEG studies is that current MEG systems mainly consist of gradiometers that are designed to focus on near-field activity (i.e., convexity of the cerebral cortex). Thus, attenuation of amplitude when measuring activity from deep sources is a major concern. In fact, a previous MEG study has shown that the sensitivity of MEG to amplitude decreased in deeper areas such as the Sylvian fissure, interhemispheric areas, and ventral parts of the brain (Goldenholz et al., 2009). Overall, the *anatomical distance* affects the amplitudes of SI and SII differently. The *spatial distance* also complicates the sensitivity problem, especially in the temporal regions, because head size varies from subject to subject while the sensor helmet is a fixed-size. Therefore, the distance between scalp and sensors in the temporal regions is sometimes not negligible. Thus, in light of the above, we admit that the SEF results should be interpreted carefully. Computation of dipole moment, which were unobtainable due to the lack of MRI in our subjects, would theoretically provide a more desirable amplitude measure, but in turn, its accuracy largely depends on how precise the MEG–MRI co-registration is as well as how precise the inverse solution can be performed. As mentioned above, we also used the amplitude-free measures to overcome the issue of amplitude measurement. Consequently, the significantly enhanced oscillatory activities, both in local and in network, validated the aging effects on SEFs.

In conclusion, our results support the presence of wide-spread cortical disinhibition across SI and SII. The oscillatory activity indices were particularly useful for weighing the effects of aging on the somatosensory system. Further studies are required to elucidate the functional impact of the age-related hypersynchrony in SII.

Acknowledgments

This study was supported in part by Grants-in-aid for Scientists, No. 19390242, No. 22390177, and No. 25870511, from the Ministry of Education, Culture, Sports, Science and Technology in Japan.

References

Barba C, Frot M, Mauguière F. Early secondary somatosensory area (SII) SEPs. Data from intracerebral recordings in humans. Clin Neurophysiol 2002;113:1778–86.
Desmedt JE, Cheron G. Somatosensory evoked potentials to finger stimulation in healthy octogenarians and in young adults: wave forms, scalp topography and transit times of parietal and frontal components. Electroencephalogr Clin Neurophysiol 1980;50:404–25.
Desmedt JE, Cheron G. Non-cephalic reference recording of early somatosensory potentials to finger stimulation in adult or aging normal man: differentiation of widespread N18 and contralateral N20 from the prerolandic P22 and N30 components. Electroencephalogr Clin Neurophysiol 1981;52:553–70.
Dinse HR, Kleibel N, Kalisch T, Ragert P, Wilimzig C, Tegenthoff M. Tactile coactivation resets age-related decline of human tactile discrimination. Ann Neurol 2006;60:88–94.
Dorfman LJ, Bosley TM. Age-related changes in peripheral and central nerve conduction in man. Neurology 1979;29:38–44.
Drechsler F. Quantitative analysis of neurophysiological processes of the aging CNS. J Neurol 1978;218:197–213.
Goldenholz DM, Ahlfors SP, Hämäläinen MS, Sharon D, Ishitobi M, Vaina LM, et al. Mapping the signal-to-noise-ratios of cortical sources in magnetoencephalography and electroencephalography. Hum Brain Mapp 2009;30:1077–86.
Hagiwara K, Okamoto T, Shigeto H, Ogata K, Somehara Y, Matsushita T, et al. Oscillatory gamma synchronization binds the primary and secondary somatosensory areas in humans. Neuroimage 2010;51:412–20.
Hari R, Forss N. Magnetoencephalography in the study of human somatosensory cortical processing. Philos Trans R Soc Lond B Biol Sci 1999;354:1145–54.
Hashimoto I, Mashiko T, Imada T. Somatic evoked high-frequency magnetic oscillations reflect activity of inhibitory interneurons in the human somatosensory cortex. Electroencephalogr Clin Neurophysiol 1996;100:189–203.
Hashimoto I. High-frequency oscillations of somatosensory evoked potentials and fields. J Clin Neurophysiol 2000;17:309–20.
Huttunen J, Wikstrom H, Salonen O, Ilmoniemi RJ. Human somatosensory cortical activation strengths: comparison between males and females and age-related changes. Brain Res 1999;818:196–203.
Kakigi R, Hoshiyama M, Shimojo M, Naka D, Yamasaki H, Watanabe S, et al. The somatosensory evoked magnetic fields. Prog Neurobiol 2000;61:495–523.
Kalisch T, Ragert P, Schwenkreis P, Dinse HR, Tegenthoff M. Impaired tactile acuity in old age is accompanied by enlarged hand representations in somatosensory cortex. Cereb Cortex 2009;19:1530–8.
Karhu J, Tesche CD. Simultaneous early processing of sensory input in human primary (SI) and secondary (SII) somatosensory cortices. J Neurophysiol 1999;81:2017–25.
Kida T, Wasaka T, Inui K, Akatsuka K, Nakata H, Kakigi R. Centrifugal regulation of human cortical responses to a task-relevant somatosensory signal triggering voluntary movement. Neuroimage 2006;32:1355–64.
Kida T, Inui K, Wasaka T, Akatsuka K, Tanaka E, Kakigi R. Time-varying cortical activations related to visual-tactile cross-modal links in spatial selective attention. J Neurophysiol 2007;97:3585–96.
Lin YY, Forss N. Functional characterization of human second somatosensory cortex by magnetoencephalography. Behav Brain Res 2002;135:141–5.
Mazzola L, Isnard J, Mauguière F. Somatosensory and pain responses to stimulation of the second somatosensory area (SII) in humans. A comparison with SI and insular responses. Cereb Cortex 2006;16:960–8.
Nakano S, Hashimoto I. The later part of high-frequency oscillations in human somatosensory evoked potentials is enhanced in aged subjects. Neurosci Lett 1999;276:83–6.
Oostenveld R, Fries P, Maris E, Schoffelen JM. FieldTrip: open source software for advanced analysis of MEG, EEG, and invasive electrophysiological data. Comput Intell Neurosci 2011;2011:156869.
Ozaki I, Hashimoto I. Exploring the physiology and function of high-frequency oscillations (HFOs) from the somatosensory cortex. Clin Neurophysiol 2011;122:1908–23.
Palva S, Linkenkaer-Hansen K, Näätänen R, Palva JM. Early neural correlates of conscious somatosensory perception. J Neurosci 2005;25:5248–58.
Raij T, Karhu J, Kicić D, Lioumis P, Julkunen P, Lin FH, et al. Parallel input makes the brain run faster. Neuroimage 2008;40:1792–7.
Simões C, Jensen O, Parkkonen L, Hari R. Phase locking between human primary and secondary somatosensory cortices. Proc Natl Acad Sci USA 2003;100:2691–4.
Sinkkonen J, Tiitinen H, Näätänen R. Gabor filters: an informative way for analysing event-related brain activity. J Neurosci Methods 1995;56:99–104.

Stam CJ, Nolte G, Daffertshofer A. Phase lag index: assessment of functional connectivity from multi channel EEG and MEG with diminished bias from common sources. Hum Brain Mapp 2007;28:1178–93.
Stephen JM, Ranken D, Best E, Adair J, Knoefel J, Kovacevic S, et al. Aging changes and gender differences in response to median nerve stimulation measured with MEG. Clin Neurophysiol 2006;117:131–43.
Tanosaki M, Ozaki I, Shimamura H, Baba M, Matsunaga M. Effects of aging on central conduction in somatosensory evoked potentials: evaluation of onset versus peak methods. Clin Neurophysiol 1999;110:2094–103.
Taulu S, Simola J. Spatiotemporal signal space separation method for rejecting nearby interference in MEG measurements. Phys Med Biol 2006;51:1759–68.
Turman AB, Morley JW, Zhang HQ, Rowe MJ. Parallel processing of tactile information in cat cerebral cortex: effect of reversible inactivation of SII on SI responses. J Neurophysiol 1995;73:1063–75.
Vinck M, Oostenveld R, van Wingerden M, Battaglia F, Pennartz CM. An improved index of phase-synchronization for electrophysiological data in the presence of volume-conduction, noise and sample-size bias. Neuroimage 2011;55:1548–65.
Wood CC, Cohen D, Cuffin BN, Yarita M, Allison T. Electrical sources in human somatosensory cortex: identification by combined magnetic and potential recordings. Science 1985;227:1051–3.
Zhang HQ, Murray GM, Turman AB, Mackie PD, Coleman GT, Rowe MJ. Parallel processing in cerebral cortex of the marmoset monkey: effect of reversible SI inactivation on tactile responses in SII. J Neurophysiol 1996;76:3633–55.
Zhang HQ, Zachariah MK, Coleman GT, Rowe MJ. Hierarchical equivalence of somatosensory areas I and II for tactile processing in the cerebral cortex of the marmoset monkey. J Neurophysiol 2001a;85:1823–35.
Zhang HQ, Murray GM, Coleman GT, Turman AB, Zhang SP, Rowe MJ. Functional characteristics of the parallel SI- and SII-projecting neurons of the thalamic ventral posterior nucleus in the marmoset. J Neurophysiol 2001b;85:1805–22.

NEUROPATHOLOGY

Neuropathology 2014; **34**, 555–570 doi:10.1111/neup.12143

Symposium: Definition and Differentials – How to Distinguish Disease-Specific Changes on Microscopy

Astrocytic inclusions in progressive supranuclear palsy and corticobasal degeneration

Mari Yoshida

Institute for Medical Science of Aging, Aichi Medical University, Aichi, Japan

Tufted astrocytes (TAs) in progressive supranuclear palsy (PSP) and astrocytic plaques (APs) in corticobasal degeneration (CBD) have been regarded as the pathological hallmarks of major sporadic 4-repeat tauopathies. To better define the astrocytic inclusions in PSP and CBD and to outline the pathological features of each disease, we reviewed 95 PSP cases and 30 CBD cases that were confirmed at autopsy. TAs exhibit a radial arrangement of thin, long, branching accumulated tau protein from the cytoplasm to the proximal processes of astrocytes. APs show a corona-like arrangement of tau aggregates in the distal portions of astrocytic processes and are composed of fuzzy, short processes. Immunoelectron microscopic examination using quantum dot nanocrystals revealed filamentous tau accumulation of APs located in the immediate vicinity of the synaptic structures, which suggested synaptic dysfunction by APs. The pathological subtypes of PSP and CBD have been proposed to ensure that the clinical phenotypes are in accordance with the pathological distribution and degenerative changes. The pathological features of PSP are divided into 3 representative subtypes: typical PSP type, pallido-nigro-luysian type (PNL type), and CBD-like type. CBD is divided into three pathological subtypes: typical CBD type, basal ganglia- predominant type, and PSP-like type. TAs are found exclusively in PSP, while APs are exclusive to CBD, regardless of the pathological subtypes, although some morphological variations exist, especially with regard to TAs. The overlap of the pathological distribution of PSP and CBD makes their clinical diagnosis complicated, although the presence of TAs and APs differentiate these two diseases. The characteristics of tau accumulation in both neurons and glia suggest a different underlying mechanism with regard to the sites of tau aggregation and fibril formation between PSP and CBD: proximal-dominant aggregation of TAs and formation of filamentous NFTs in PSP in contrast to the distal-dominant aggregation of APs and formation of less filamentous pretangles in CBD.

Key words: astrocytic plaque, corticobasal degeneration, fibril formation, progressive supranuclear palsy, tufted astrocyte.

INTRODUCTION

Progressive supranuclear palsy (PSP)[1] and corticobasal degeneration (CBD)[2] have been regarded as distinct clinicopathological entities with hyperphosphorylated four repeat (4R) tau aggregation in neurons and glia, although the recent recognitions of many clinical similarities have increasingly raised more difficulties in the clinical diagnosis of these two disorders. However, microscopic cellular tau pathology has been used to distinguish PSP from CBD.[3–5] PSP is defined primarily by tau-positive neurofibrillary tangles (NFTs), coiled bodies, threads, and tufted astrocytes, in contrast to the ballooned neurons, pretangles, threads, and astrocytic plaques that are characteristic of CBD (Table 1). Because PSP and CBD frequently present similar pathological distributions (Table 1, Fig. 1), a pathological diagnosis may be difficult without the discrimination of abnormal tau inclusions and particularly of the most characteristic and obvious tau morphology, that of astrocytic inclusions.[6] Therefore, it is important to reevaluate and differentiate between tufted astrocytes (TAs) and astrocytic plaques (APs) and to discuss the pathogenesis of these types of inclusions. To address these issues, we reviewed the morphology and differential distribution of

Correspondence: Yoshida Mari, MD, PhD, Institute for Medical Science of Aging, Aichi Medical University, 1-1 Yazakokarimata, Nagakute, Aichi 480-1195, Japan. Email: myoshida@aichi-med-u.ac.jp

Received 16 April 2014; revised 15 June 2014 and accepted 15 June 2014.

Table 1 Diagnostic pathological findings in progressive supranuclear palsy (PSP) and corticobasal degeneration (CBD)

	PSP	CBD
Lesion	Distribution	
Neuronal loss & gliosis	Affected cortices (variable)	Affected cortices/subcortical white matter (gliosis)
	Globus pallidus	Globus pallidus (variable)
	Subthalamic nucleus	Subthalamic nucleus (variable)
	Substantia nigra	Substantia nigra
		Striatum (caudate and putamen) (gliosis)
	Brainstem tegmentum	Brainstem tegmentum (variable)
	Dentate nucleus	Dentate nucleus (variable)
	Pons and medulla (variable)	Pons and medulla (variable)
Ballooned or achromatic neurons		Affected cortices
Gallyas/4R-tau positive lesions		
Neuronal inclusions	NFTs > Pretangles	Pretangles >> NFTs
	Substantia nigra, oculomotor complex, locus ceruleus, pons, brainstem nuclei, dentate nucleus, globus pallidus, subthalamic nucleus	Affected cortices, substantia nigra, globus pallidus, subthalamic nucleus
	Striatum, thalamus, basal nucleus of Meynert	Striatum, thalamus, basal nucleus of Meynert
	Affected Cortices (variable)	Brainstem nuclei and dentate nucleus
	Spinal cord	Spinal cord
Threads and coiled bodies	Threads and coiled bodies	Threads >> coiled bodies
	Brainstem, cerebellar white matter, globus pallidus, subthalamic nucleus, striatum, thalamus, gray matter and white matter, spinal cord	Subcortical white matter and gray matter, globus pallidus, subthalamic nucleus, striatum, thalamus, brainstem, spinal cord
Astrocytic inclusions	Tufted astrocytes	Astrocytic plaques
	Affected cortices, striatum, brainstem	Affected cortices, striatum

4R-tau, 4 repeat tau; NFTs, neurofibrillary tangles.

pathologic lesions of 95 neuropathologically confirmed PSP cases and 30 CBD cases that were registered at the Institute for Medical Science of Aging, Aichi Medical University. Our focus was on the pathogenesis of astrocytic inclusions, their disease specificity, and their morphological variations.

PROGRESSIVE SUPRANUCLEAR PALSY (PSP)

PSP is a progressive neurodegenerative disorders, described by Steele, Richardson and Olszewski in 1964.[1] It is the second most common form of parkinsonism after Parkinson's disease. Clinical features include abnormal gait, and postural instability, and recurrent falls, supranuclear ophthalmoparesis, cognitive and behavioral changes, pseudobulbar features and dystonia.

Clinical aspects

As noted previously, pathologically confirmed cases of PSP have exhibited some variation of the clinical and pathological features. Therefore, clinical subtypes were proposed to classify PSP: PSP-Richardson, PSP-parkinsonism (PSP-P),[7,8] PSP-pure akinesia with gait freezing (PSP-PAGF),[9] PSP-primary progressive aphasia,[10,11] and PSP-predominant cerebellar involvement (PSP-C).[12,13] The PSP-Richardson type is the prototypical form of PSP that is defined by early falls, early cognitive dysfunction, abnormalities of gaze and postural instabilities. PSP-P represents asymmetric onset, tremor, early bradykinesia, non-axial dystonia and a response to levodopa. Individuals with PSP-PAGF present with the gradual onset of freezing of gait or speech, absent limb rigidity and tremor, a lack of sustained response to levodopa, and no dementia or ophthalmoplegia in the first 5 years of disease. PSP-primary progressive aphasia is defined by the presence of primary progressive aphasia, or progressive nonfluent aphasia. Individuals with PSP-C develop cerebellar-predominant ataxia as the initial and principal symptom.

Neuropathology

Neuropathological diagnostic criteria

The pathological criteria for the diagnosis of PSP are well established and include specific neuronal loss with gliosis and neurofibrillary tangles (NFTs) in the subcortical and brainstem nuclei and in the cerebellar dentate nucleus with the pathological accumulation of abnormally phosphorylated microtubule-associated protein tau into filamentous deposits.[14] The NINDS diagnostic criteria for PSP and related disorders are pertinent for typical PSP,

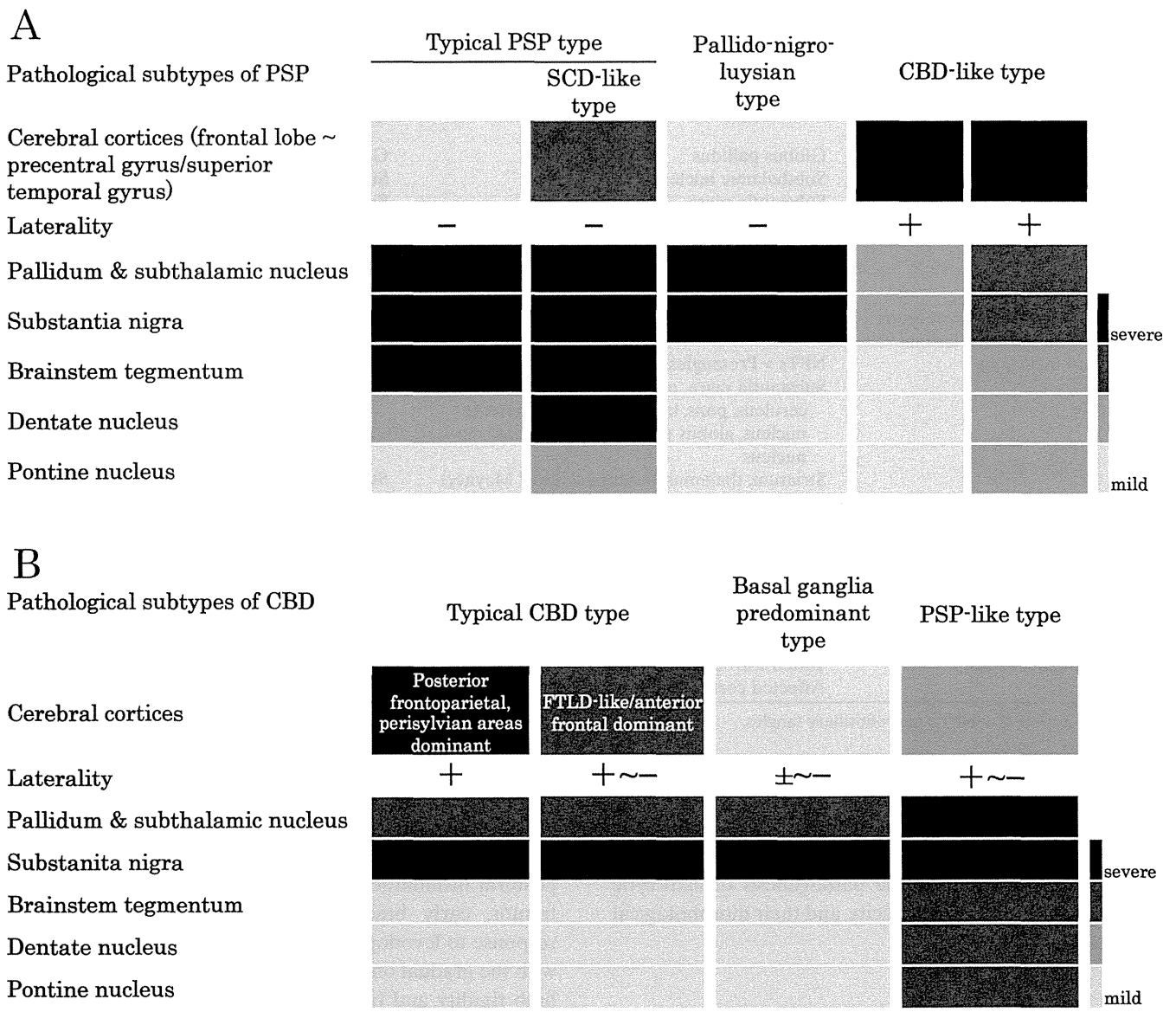

Fig. 1 The group of pathological subtypes in PSP (A) and CBD (B). (A) The pathological subtypes in PSP is generally divided into three representative types: typical PSP type, pallido-nigro-luysian type (PNL type), and CBD-like type, according to the distribution of the lesions and the severity. The spinocerebellar degeneration (SCD)-like type is associated with severe degeneration of the dentate nucleus, superior cerebellar peduncles, cerebellar cortex, white matter and pontine tegmentum and base, which are frequently associated with frontal involvement. The PNL type shows relatively restricted changes in pallido-nigro-luysian lesions. The CBD-like type is accompanied by more severe, asymmetrical cortical changes and a variable degeneration of the basal ganglia, brainstem and cerebellar dentate nucleus. (B) The pathological subtypes of CBD is generally divided into three representative types: typical CBD type, basal ganglia-predominant type, and PSP-like type, according to the distribution of the lesions and the severity. The typical CBD type shows dominant cortical involvement with laterality in the posterior frontoparietal or perisylvian areas. Some cases exhibit anterior frontal-dominant cortical degeneration, such as frontotemporal lobar degeneration. The basal ganglia-predominant type reveals severe involvement of the pallidum and subthalamic nucleus, with relatively mild cortical degeneration without distinct laterality. The PSP-like type shows severe degeneration of the brainstem and dentate nucleus similar to that seen in PSP, in addition to the variable cortical involvement.

which conforms to the original description, and atypical PSP, which consists of histologic variants where the severity or distribution of abnormalities, or both, deviate from the typical pattern; these criteria are also relevant for combined PSP, in which typical PSP is accompanied by concomitant infarcts in the brainstem, basal ganglia, or both.[3,12] Microscopic findings include a high density of NFTs and neuropil threads in at least three of the following areas: the pallidum, subthalamic nucleus, substantia nigra, or pons. In addition, a low to high density of NFTs or neuropil threads is found in at least three of the following areas: the striatum, oculomotor complex, medulla, or dentate nucleus. A clinical history

that is compatible with PSP is also required for diagnosis according to this set of criteria. These criteria have come to define the typical clinicopathological PSP cases. However, based on these criteria, it was recommended that atypical PSP should be excluded as a PSP subtype because further neuropathological studies of this entity were needed.

Neuropathological reevaluation of PSP cases

Among 95 pathologically confirmed PSP cases, 25 cases were associated with other significant diseases. Two of these cases were associated with Alzheimer's disease, 12 with Parkinson's disease or dementia with Lewy bodies (DLB), 1 with multiple system atrophy, 1 with SCA6 and DLB, 1 with amyotrophic lateral sclerosis, 1 with traumatic brain injury, 4 with cerebrovascular disease, 1 with glioblastoma, and 2 cases were without detailed information. With the exception of these 25 cases, 70 cases were analyzed and had the following characteristics: a mean age at onset of 67 years (range 39–92 years), a mean disease duration of 8 years (range 1–28 years), and a mean age at death of 75 years (range 49–106 years). PSP is a sporadic disease, although approximately 7% of affected individuals have a family history of neurological disorders, including parkinsonism or dementia.

Macroscopic and microscopic findings

The macroscopic examination of the brain in typical PSP reveals mild frontal atrophy including precentral gyrus, particularly in the convexity (Fig. 2A). The brainstem and cerebellum are mildly atrophic. The globus pallidus and subthalamic nucleus usually show a brownish atrophy. The third ventricle may be enlarged. The tegmentum of the midbrain and pons also shows atrophy. The substantia nigra shows discolored, while the locus ceruleus is often relatively preserved. The cerebellar dentate nucleus, and the superior cerebellar peduncle are atrophic.

The microscopic findings indicate neuronal loss and gliosis with NFTs, which appear globose in appearance, in the basal ganglia, thalamus, brainstem, and cerebellum (Table 1, Fig. 3). The thalamus has mild to moderate neuronal loss and gliosis, while the putamen and the caudate show mild gliosis. The most affected nuclei are the globus pallidus, subthalamic nucleus and substantia nigra. The affected regions of the brainstem are as follows: midbrain tegmentum including the superior colliculus, periaqueductal gray matter, oculomotor nuclei, locus ceruleus, pontine tegmentum, pontine nuclei, medullary tegmentum and the inferior olivary nucleus. The dentate nucleus usually exhibits grumose degeneration. The superior cerebellar peduncles are atrophic, and the cerebellar cortex may show mild loss of Purkinje cells with mild atrophy of the white matter. The medullary tegmentum may be atrophic with myelin pallor. The cerebral cortices show mild gliosis especially in the premotor and precentral gyrus in the convexity. The spinal cord, especially the cervical segment, is usually involved, particularly in the medial division of the anterior horn and intermediate gray matter.[15–17] Transverse sections of the spinal cord often show myelin pallor in the anterolateral funiculus in the cervical and thoracic segments. Immunohistochemistry for phosphorylated tau or modified Gallyas silver staining reveals NFTs, pretangles in neurons, tufted astrocytes, coiled bodies in oligodendrocytes, and threads (Table 1, Fig. 3).

Tufted astrocytes

TAs are defined as radial arrangements of thin and long branching fibers without collaterals that course continuously through the cytoplasm to the distal processes of astrocytes (Fig. 3d–j,m,n).[6,18] "Tufts of abnormal fiber," as described in PSP by Hauw *et al.*,[19] is the root of the nomenclature for "tufted astrocytes," although their cellular characterization was not mentioned in their study. Tufted astrocytes were described by Hauw *et al.*[19] as star-like tufts of fibers devoid of degenerative features and without amyloid cores that are clearly distinguishable with Bodian stain as well as with tau immunocytochemistry. The astrocytic nature of the cells that contain the tufted-type inclusions was confirmed by the double-labeling of sections with antibodies to GFAP, CD44 and abnormal tau.[20–22] Cytoplasmic staining is usually not conspicuous within TAs

Fig. 2 Macroscopic findings of typical PSP type (A), pallido-nigro-luysian (PNL)- type (B) and CBD-like type (C).
(A) Macroscopic findings in coronal sections of typical PSP show mild frontal atrophy in the convexity (a), atrophy of the pallidum and subthalamic nucleus (a, arrow), atrophy of the brainstem tegmentum (b), loss of pigment in the substantia nigra (b, arrow) with preservation of pigment in the locus ceruleus, and atrophy of the cerebellar dentate nucleus (c). Bar = 2 cm.
(B) Macroscopic findings in PNL-type PSP reveal severe atrophy of the pallidum and the subthalamic nucleus (a) and depigmentation of the substantia nigra (b), with relative preservation of the brainstem tegmentum (b) and cerebellar dentate nucleus (c). The PNL-type sometimes shows atypical TAs, which demonstrates proximal dominant tau accumulations (d, e). d, Gallyas silver stain; e, AT8 immunohistochemistry; a, b, c, bar = 2 cm; e, bar = 10 μm.
(C) Macroscopic findings in CBD-like type PSP indicate left side-predominant degeneration of the cerebral cortices and the basal ganglia (a–d) with relatively mild atrophy of the brainstem (e). Microscopically typical TAs are observed in the basal ganglia and cerebral cortices (f, g). a, c, Klüver-Barrera stain; b, d, Holzer stain; f, Gallyas silver stain; g, AT8 immunohistochemistry; bar = 10 μm.